Electron-induced vibrational excitation of CO_2 in dc electric and magnetic fields

Mirjana M. Vojnović,[1,*] Miroslav M. Ristić,[2] Violeta V. Stanković,[1] and Goran B. Poparić[1]
[1]*University of Belgrade, Faculty of Physics, Studentski Trg 12, P.O. Box 44, 11000 Belgrade, Serbia*
[2]*University of Belgrade, Faculty of Physical Chemistry, Studentski Trg 12, P.O. Box 47, 11000 Belgrade, Serbia*

(Received 25 February 2019; revised manuscript received 9 May 2019; published 28 June 2019)

In the present study rate coefficients for vibrational excitation of CO_2 gas molecules by electrons in the presence of uniform electric and magnetic fields are investigated. Calculations are performed for transition from the ground state to each of the symmetric, asymmetric, and bending vibrational states. A Monte Carlo simulation is used to produce nonequilibrium electron energy distribution functions. Results are obtained for the electric field over gas number density ratio, E/N, ranging from 20 to 1000 Td, and for the magnetic field over gas number density ratio, B/N, with values of 0, 1000, 2000, and 3000 Hx.

DOI: 10.1103/PhysRevE.99.063211

I. INTRODUCTION

The continuous increase of CO_2 emission in the Earth's atmosphere originating from fossil fuel combustion has led to increasing efforts to find a solution to the global warming problem. This has made the carbon dioxide molecule a high priority in many plasma technology and scientific studies, including studies of particle collisions.

There is a great interest of plasma technologies in conversion of the CO_2 molecule to renewable chemical energy sources to reduce both the usage of fossil fuels and the consequential CO_2 emission in the atmosphere [1–3]. The chain of events in the process of CO_2 conversion to these, so-called, solar fuels is triggered by the electron impact dissociation of the CO_2 molecule. It is, therefore, a matter of great importance to achieve high-energy efficiency in this initial process [4]. Since direct electron impact dissociation requires acceleration of electrons to relatively high energies, which involves high-energy losses, researchers have focused on the idea of using cold plasma to enhance the dissociation rate through electron impact vibrational excitations [5–7]. The energy efficiency of CO_2 dissociation in low-temperature plasma is highest if CO_2 decomposition is accomplished by nonadiabatic transition from the ground state $^1\Sigma^+$ to $^3B_2$ at the point of the term crossing, which is stimulated by step-by-step vibrational excitation that occurs as a result of vibration-vibration quantum exchange [8,9]. Vibrational energy for this transition is lower than energy required for dissociation by electronic excitation [9]. Another dissociation pathway of desirable energy efficiency takes place when a single vibrational excitation in the electronic ground state is sufficient for nonadiabatic term crossing [2]. The process of vibrational excitation in low-temperature plasma predominantly leads to CO_2 molecular dissociation, among all the other processes, due to the high potential for energy storage of vibrationally excited molecules [5].

The complete knowledge of vibrational excitation rate coefficients for each mode of vibration (symmetric, asymmetric, and bending) is of great value in the development of plasma models in studies aimed at CO_2 dissociation processes in an attempt to fully understand the mechanism behind vibrationally assisted splitting of this molecule and to find the best working conditions to optimize energy efficiency. Few studies have provided vibrational excitation rate coefficients under nonequilibrium conditions [6,10]. In research performed by our group in 2010 [11] we also dealt with vibrational excitation of the CO_2 molecule through the calculation of electron energy transfer rate coefficients.

These studies took into account the presence of only the electric field. However, discharge devices that produce plasmas often use the magnetic field to confine electrons in order to increase the discharge efficiency. The electron confinement is maximal in an orthogonal configuration of electric and magnetic fields [12]. It has been shown that the presence of the magnetic field enhances the energy efficiency of the conversion process, since the increased electron density improves the CO_2 dissociation [13]. With the knowledge that vibrational excitation plays a significant role under nonequilibrium conditions, one cannot omit to access the analysis of the vibrational rate coefficients' change in shape and intensity with magnetic field application and with the change of its magnitude. Furthermore, vibrational rate values obtained for the case of the inclusion of the magnetic field would be a valuable set of input data for future models of low-temperature CO_2 plasma. Hence, we conducted calculations to obtain a more complete set of rate coefficients than before for excitation from the ground state of carbon dioxide to different vibrational modes in the presence of both the electric and the magnetic fields. Most of the cross sections for vibrational excitation we used in our study are experimentally obtained values, whereby the major part (excitations of the symmetric stretch modes for $v = 1$ to 8) consists of earlier measurements by our group [11]. We used those data to calculate rate coefficients and separate individual contributions to overall vibrational excitation. We expect the results we obtained to be very useful for more general applications in plasma

*mvojnovic@ff.bg.ac.rs

models. For example, our data are relevant for the development of models simulating the CO_2-rich atmosphere of Mars where dissociation also occurs via excitation of vibrational modes [14].

Nonequilibrium electron energy distribution functions (EEDFs) were generated by a Monte Carlo simulation of electron transport through CO_2 gas. The simulation was used in our earlier work on the carbon dioxide molecule [11], and it has been upgraded since then to include the presence of the magnetic field [15,16].

Superelastic collisions are not included in our simulation. This is justified bearing in mind that the lowest value of the reduced electric field, E/N, in our calculations is still beyond the range in which superelastic collisions with thermally excited molecules play an important role. It has been estimated that superelastic collisions make significant changes in the shape of EEDFs for E/N values from 1 to 10 Td and below [17,18].

II. MONTE CARLO SIMULATION

A. The procedure description

Initially, electrons are at rest at the origin. Electrons start their motion one at a time in the direction of the electric field **E** with a nonzero value of kinetic energy. The Lorentz force appearing due to magnetic field presence acts upon electrons, changing their path. The differential equation of electron motion reads

$$m\frac{d^2\mathbf{r}}{dt^2} = e\left(\mathbf{E} + \frac{d\mathbf{r}}{dt} \times \mathbf{B}\right), \tag{1}$$

where **r** is radius vector of the electron, and m and e are the electron's mass and charge, respectively. The full analytical solutions of the equation given above are used for calculation of the electron's position and velocity in each subsequent time step [19,20].

While passing through a gas, the electron occasionally suffers collisions with molecules, which are at their ground rotational, vibrational, and electronic state. Whether there will be a collision at all, and if so, of what kind, is determined by generating a pseudorandom number weighted by the probability of the given process. The probability of a collision process is related to the integral cross section (ICS) of the process. ICSs for all scattering events are experimentally or theoretically obtained values, contained in the database that our program uses as input data.

The database of the simulation also contains experimentally measured differential cross sections (DCSs) for elastic scattering, which were used to determine the angular distribution of scattered electrons. The input data are first dynamically interpolated for the actual electron kinetic energy value. Afterwards, a random number is generated to provide the scattering angle. The data previously obtained after interpolation with respect to energy are then used to interpolate for each randomly generated angle. Since elastic collision processes predominate over inelastic processes, accurate knowledge of elastic DCSs is required for generating proper angular distribution in the simulation. Angular distributions for inelastic processes, which are much less frequent, were treated as isotropic.

In an inelastic collision, an electron loses part of its energy equal to the threshold energy of the ongoing collision process. In the case of ionization, this energy loss is shared between the ejected electron and the impinging electron in the ratio that is determined by the generated pseudorandom number. The information of the ejected electron's position and velocity is stored in the computer memory for the future tracking of its evolution after all primary electrons are processed. If the electron is attached to a molecule the simulation simply skips to a new electron from the sample.

The number of electrons tracked in the simulation was about 10^7 for each choice of the parameters. The electron-electron interaction is omitted; the low electron density approximation is justified considering that the ionization degree is not very high.

The gas pressure in the simulation was 5 Torr (667 Pa), which corresponds to the CO_2 molecule number density of $N = 1.61 \times 10^{23}\,\mathrm{m}^{-3}$. At higher pressures when collisions of neutral atoms and molecules become significant, vibrational distribution in CO_2 gets to be complex. For those cases macroscopic models (multitemperature approach, two-level distribution) have been developed, which are alternative to the demanding state-to-state model [21].

After many subsequent collisions, the dissipated energy is nearly equalized to the energy the electrons have gained upon acceleration under the influence of the electric field. In other words, the mean electron energy is stabilized around some value and a steady state is established. This is the time when all necessary transport parameters are being sampled at each time step, the mean electron energy and the EEDF in the first place. To shorten the simulation time, we set the initial kinetic energy value to be similar to the expected value, which we had first determined after several trial runs.

Prior to use for obtaining new results, the simulation code was tested by implementing the corresponding model gas in the simulation and comparing the resulting electron transport coefficients with values of benchmark calculations. In these tests we used the Reid model gas [22] for conservative collision processes and the modified Ness-Robson model gas [23] for nonconservative collision processes (ionization and electron attachment). Since benchmark calculations by Nolan *et al.* [23] treat ionization and attachment separately, the combined ionization and attachment collision processes simulated with our code have been tested by comparing the obtained results with ones obtained by using BOLSIG+ software, version 03/2016 [24], with the Ness-Robson model gas [23] as input cross-section database and parameters set to include both kinds of nonconservative collision processes.

B. The cross-section set

Our cross section (CS) database consists of CSs for elastic scattering, vibrational and electronic state excitation, dissociative attachment, and ionization. Dissociation of CO_2 is implicitly included in the simulation through excitation of predissociative electronic and vibrational states and dissociative attachment.

Table I presents the CSs we used, along with the threshold energy for the given process and references. CSs from Table I are shown in Fig. 1. By summing all of the CSs given in

TABLE I. Cross sections used for electron impact excitation of the CO_2 molecule with the indicated thresholds in eV and references.

Scattering process	Excited state	Threshold	Ref.
Elastic	–	–	[28–30]
Vibrational excitation	(100)	0.172	[11]
	(200)	0.3441	[11]
	(300)	0.510	[11]
	(400)	0.6882	[11]
	(500)	0.860	[11]
	(600)	1.0323	[11]
	(700)	1.204	[11]
	(800)	1.3764	[11]
	(1000)	1.644	[34]
	(001)	0.291	[25,35,36]
	(010)	0.082	[25,35,36]
	(020)	0.165	[36–38]
	(040)	0.331	[37,38]
	(120)	0.337	[37,38]
	(030)+(110)	0.252	[18]
	(050)+(210)+(130) +(021)+(101)	0.422	[18]
Excitation of electronic states	$^1\Pi_u$	11.385	[31]
	$^1\Sigma_u^+$	11.048	[31]
	7 eV excitation	7	[24,39]
Ionization	–	13.769	[25,40]
Dissociative attachment	–	3.4	[25,41]

Table I, we calculated total CSs for electron scattering from the CO_2 molecule. Comparison of the obtained values to those recommended by Itikawa [25], which are based on experimental results of several different authors, showed that there was a slight discrepancy of these CSs in the energy range from approximately 10 eV up to 60 eV (Fig. 1). This is the energy interval of the electronic excitation. Electronic excitation data for CO_2 have not been fully determined in the previous studies and there is no consensus on this matter [25]. Eight of the ten electronic states for which CSs can be found in the literature are the result of theoretical studies [26,27], for which no experimental support has yet been achieved. Moreover, there is a non-negligible mismatch when these theoretical results are compared to each other. We, therefore, added in our base excitation CSs with a threshold value of 10 eV, obtained after subtraction of the summed ICSs in Table I from the total cross sections given by Itikawa [25]. In this way we obtained an excellent agreement between our transport coefficients and transport parameters measured by other authors, as shall soon be shown. These cross sections are thus equal to the contribution which is lacking in the literature and are labeled in Fig. 1 by "10 eV exc.".

The data for elastic scattering were based on several experimental measurements. At 0.155 and 1.05 eV we used values obtained in the crossed-beam experiment by Kochem *et al.* [28]. In the interval from 1.5 to 100 eV we adopted values by Tanaka *et al.* [29], except at 40, 50, 70, 80, and 90 eV where the experimental values of Kanik *et al.* [30] were used, whose CSs agree well with the values of Tanaka *et al.* [29].

We used integral cross sections for electron impact excitation of $^1\Sigma_u^+$ and $^1\Pi_u$ states from Kawahara *et al.* [31]. They derived ICSs for excitation of these states from their earlier measurements of absolute differential cross sections in crossed-beam experiments at Sophia University and at Flinders University [32] and from generalized oscillator strength data from Klump and Lassettre [33]. They also calculated ICSs for these states by using the BEf-scaling approach. The comparison they made showed consistency of calculated values with these experimental results to within experimental uncertainties. The values we adopted are those based on experimental measurements.

We also used cross sections for electronic excitation with an onset of 7 eV from the BOLSIG+ database. Cross sections for this state originate from swarm-derived analysis by Hake and Phelps [39]. According to Polak and Slovetsky [42], these cross sections comprise the contribution of seven electronic states: $^3\Sigma_u^+$, $^3\Pi_g$, $^3\Delta_u$, $^1\Pi_g$, $^3\Sigma_u^-$, $^1\Sigma_u^-$, and $^1\Delta_u$, all of which have an energy threshold of around 8 eV.

Integral cross sections for the symmetric-stretch vibrational excitation of (100), (200), (300), (400), (500), (600), (700), and (800) modes in the resonance energy range (shown in the inset of Fig. 1) are the CSs previously measured in our laboratory on a high-resolution crossed-beam double-trochoidal electron spectrometer that uses the time-of-flight technique for separation of forward and backward scattered electrons [11]. The contribution via the virtual state below

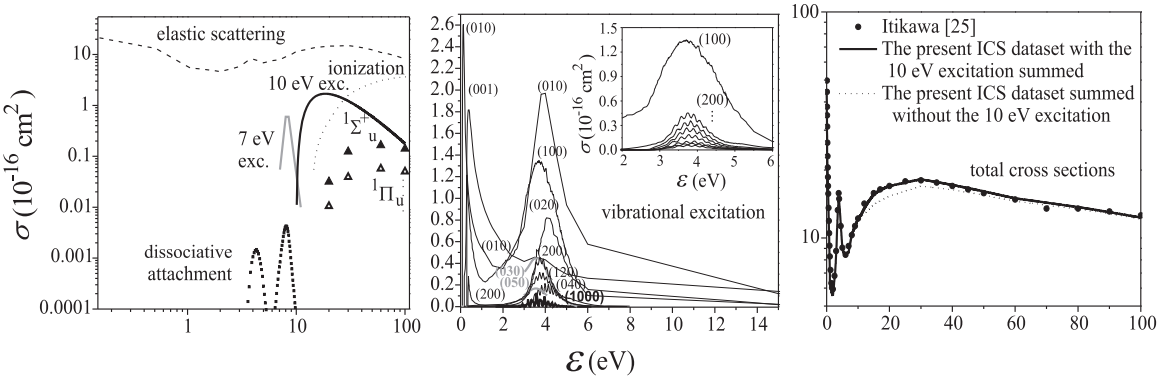

FIG. 1. Cross sections for electron collisions with CO_2. The inset shows integral cross sections for excitation of symmetric modes in the range of the resonance from earlier measurements by our group [11].

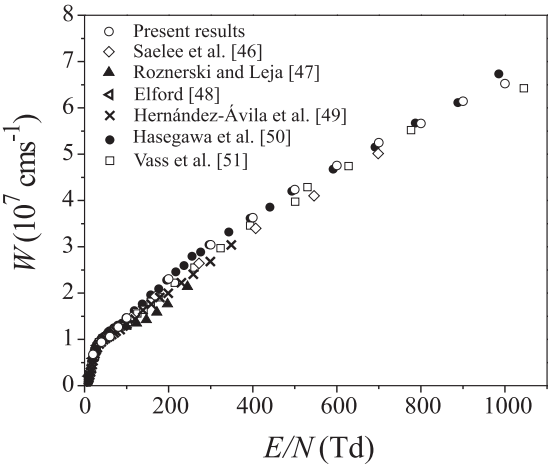

FIG. 2. Electron drift velocity vs reduced electric field.

2.5 eV was estimated on the basis of DCS measurements from Kitajima *et al.* [36] for the (100) state, and for the (200) mode the recommended values of Campbell *et al.* [37] are included, which resulted from the theoretical work of McCurdy *et al.* [38] and from the experimental results of Allan [43].

It is well known that there are couplings between some of the vibrational states of CO_2 (Fermi resonance). For example, the (100) state is coupled with the (020) state and the (200) state is coupled with the (040) and (120) modes. In order to separate the contributions of these mixed states we compared the energy loss spectra of Johnstone *et al.* [44] and Kitajima *et al.* [36] with our measurements, whereby their procedure of deconvolution of the peaks and their angular distributions were employed. In this way, the (100) and (200) modes were separated from other corresponding members of the Fermi resonance. Our DCS measurements for the (100) mode were normalized on an absolute scale at 3.8 eV by using DCSs of Kitajima *et al.* [36], which we had first extrapolated by fourth-order Legendre polynomials and integrated. Measurements for higher symmetric stretch modes were scaled on the basis of the number of counts for each vibrational mode under the same experimental conditions (see Ref. [11] for more details).

Cross sections for excitation of the (10,0,0) state originate from calculation by Laporta *et al.* [34]. The ICSs for excitation to the (001) and (010) modes in the low-energy region up to 1 eV are based on the data of Nakamura [35] obtained from a swarm experiment. For energies above 1 eV, Itikawa [25] recommended values based on experimentally obtained DCSs by Kitajima *et al.* [36]. These values were adopted fully for the (010) state and from 3 eV for the (001) state.

The ICSs for excitation to (020) and (040) bending modes and the (120) combined mode are recommended values taken from Campbell *et al.* [37]. These cross sections are based on the experimental and theoretical work of different authors: Kitajima *et al.* [36] and McCurdy *et al.* [38]. We also adopted cross sections for (030)+(110) and (050)+(210)+(130)+(021)+(101) excitations from Grofulović *et al.* [18].

For ionization processes Itikawa [25] gave recommended values from Lindsay and Mangan [40]. Their cross sections are based on time-of-flight measurements performed by Straub *et al.* [45].

Dissociative attachment CSs originate from Rapp and Briglia [41] and are recommended by Itikawa [25] in his review paper. Rapp and Briglia [41] measured absolute values of CSs for the production of O^- ions from CO_2 by using the total ionization method.

In order to test the simulation performance with the given cross section database, we compared the values of electron transport parameters obtained by our simulation with experimentally obtained results we found in literature.

Figure 2 shows the electron drift velocity dependence on the reduced electric field strength in the CO_2 gas. Drift velocity was measured by Saelee *et al.* [46], Roznerski and Leja [47], Elford [48], and Hernández-Ávila *et al.* [49] in the low and intermediate E/N range. We obtained good agreement with these values, which were measured in the energy region of low ionization. Hasegawa *et al.* [50] and Vass *et al.* [51] measured drift velocity in the entire range of E/N presented

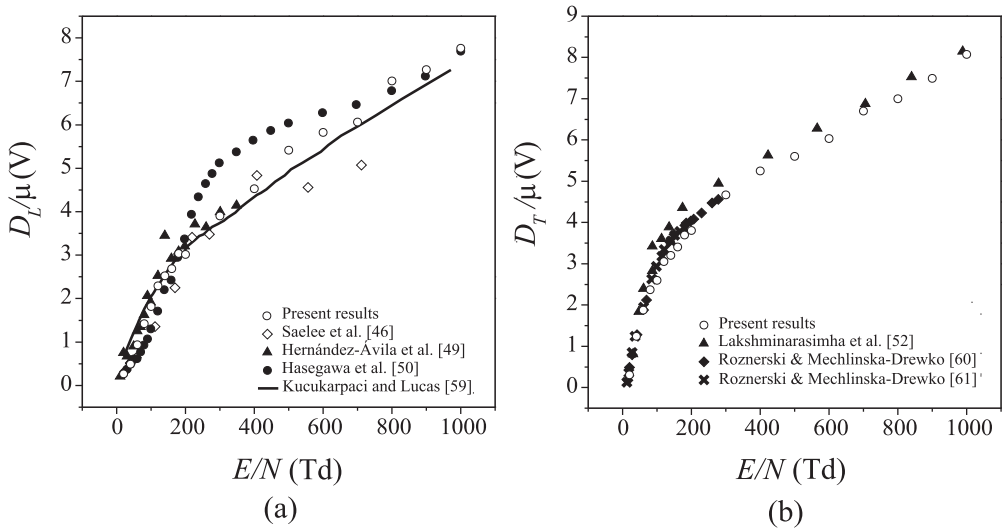

FIG. 3. Longitudinal (a) and transverse (b) diffusion coefficient to mobility vs reduced electric field.

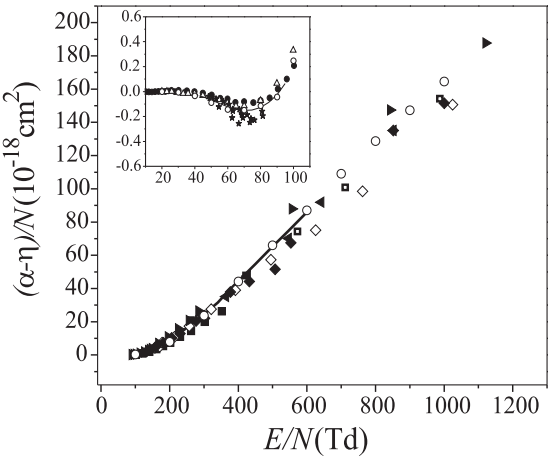

FIG. 4. Density normalized effective ionization coefficients vs reduced electric field: open circle, present results; solid square, Hernández-Ávila *et al.* [49]; open square, Lakshminarasimha *et al.* [52]; solid line, Deng and Xiao [53]; open diamond, Vass *et al.* [51]; left-facing triangle, Townsend [54]; right-facing triangle, Bhalla and Craggs [55]; and solid diamond, Schlumbohm [56]. The inset shows comparison in the low E/N range: open circle, present results; solid circle, Hernández-Ávila *et al.* [49]; open triangle, Yousfi *et al.* [57]; star, Chatterton and Craggs [58]; and solid line, Vass *et al.* [51].

here, which includes the high-energy part with considerable ionization event participation. Hasegawa and coworkers [50] used a double-shutter drift tube and Vass and coworkers [51] used a scanning drift tube apparatus to perform measurements. As can be seen, these two different experimental groups obtained very similar results and our results agree well with these measurements.

Figures 3(a) and 3(b) show that the present calculations of ratios of the longitudinal and transverse diffusion coefficients to mobility, respectively, agree well with the experimental results of different authors. Our calculations of the longitudinal diffusion coefficients deviate from measurements of Hasegawa *et al.* [50] and Saelee *et al.* [46] in the intermediate E/N range, where our values follow closely the experimental results of Hernández-Ávila [49] and the calculations of Kucukarpaci and Lucas [59]. Acceptable agreement of the present calculation of the transverse diffusion to mobility with measurements by Roznerski and Mechlińska-Drewko [60,61] and Lakshminarasimha *et al.* [52] is obtained in the whole range of the reduced electric field, with our values being closer to those of Roznerski and Mechlińska-Drewko [60,61].

In Fig. 4 our calculated values of the density normalized effective ionization coefficients $(\alpha - \eta)/N$, with α denoting the ionization coefficient and η the attachment coefficient, are compared with the experimental results of Hernández-Ávila *et al.* [49], Lakshminarasimha *et al.* [52], Vass *et al.* [51], Townsend [54], Bhalla and Craggs [55], and Schlumbohm [56] and with the calculations of Deng and Xiao [53]. The present results lie inside of this group of data. The inset in Fig. 4 presents comparison of the present results with available data in the low E/N region. Our calculations are compared with Monte Carlo calculations by Vass *et al.* [51] and with values measured by Hernández-Ávila *et al.* [49], Yousfi *et al.* [57], and Chattertron and Craggs [58]. Again, our

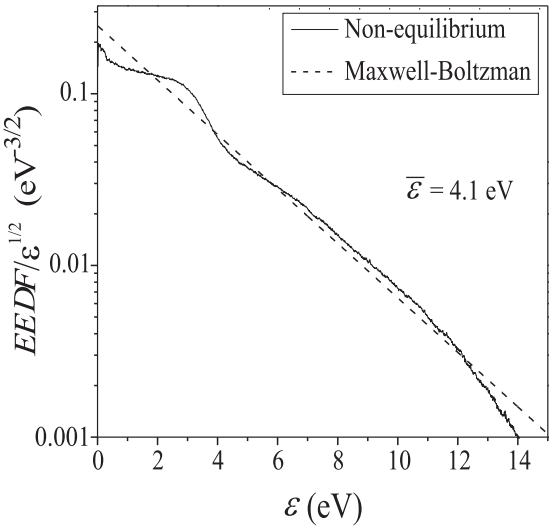

FIG. 5. Electron energy distribution function obtained by simulation at $E/N = 120$ Td and $B/N = 0$ Hx, which corresponds to a mean electron energy of 4.1 eV, compared to the Maxwell-Boltzmann distribution.

results lie inside of the experimental group of data, following closely the calculations of Vass *et al.* [51].

III. RESULTS AND DISCUSSION

Rate coefficients for a certain electron-molecule collision process, $K(\bar{\varepsilon})$, were calculated by using the following relation [62,63]:

$$K(\bar{\varepsilon}) = \sqrt{2/m} \int_{\varepsilon_{\text{th.}}}^{+\infty} \sigma(\varepsilon)\sqrt{\varepsilon} f_e(\bar{\varepsilon}, \varepsilon) d\varepsilon, \qquad (2)$$

where $\bar{\varepsilon}$ is the mean electron energy, $\sigma(\varepsilon)$ is the cross section for the considered process, $\varepsilon_{\text{th.}}$ is its threshold energy, and

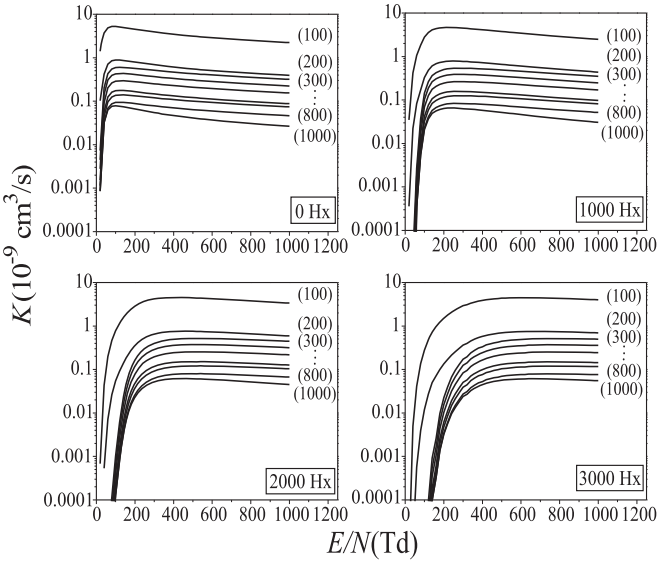

FIG. 6. Partial rate coefficients for symmetric vibrational mode excitation vs reduced electric field for various B/N values.

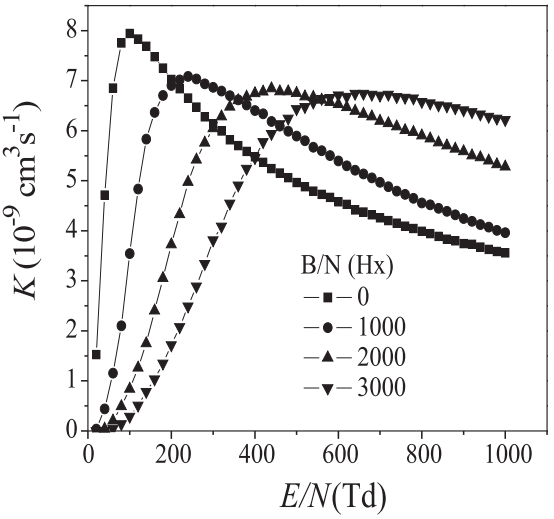

FIG. 7. Total rate coefficients for symmetric vibrational mode excitation vs reduced electric field for different reduced magnetic field values.

$f_e(\bar{\varepsilon}, \varepsilon)$ is the normalized EEDF:

$$\int_0^{+\infty} f_e(\bar{\varepsilon}, \varepsilon) d\varepsilon = 1. \tag{3}$$

EEDFs obtained by Monte Carlo simulation for different conditions were used in Eq. (2). The reduced electric field strength was varied from 20 to 1000 Td (1 Td $= 10^{-21}$ Vm^2), while the values of the reduced magnetic field strength were 0, 1000, 2000, and 3000 Hx (1 Hx $= 10^{-27}$ Tm^3). This corresponds to the mean electron energies in the interval 0–15 eV.

As an example in Fig. 5 we present EEDF obtained for $E/N = 120$ Td in the absence of the magnetic field, which we compared with the Maxwell-Boltzmann (MB) distribution for the same mean electron energy (4.1 eV). This value of the mean electron energy lies in the range of the position of resonance maxima in vibrational excitation cross sections. The EEDF is normalized according to Eq. (3) and divided by the square root of the electron energy. In the range of energies that correspond to resonance (2–6 eV) the nonequilibrium EEDF is perturbed in relation to the MB distribution.

Shapes of these EEDFs dictate the resulting rate coefficients. The results that are about to be shown are governed by the overlapping regions of EEDFs and CSs for excitation of the given state. For example, CSs that possess both the threshold peak and the resonance part make different contributions of each of these parts to the rate coefficient depending on the region that is mostly covered by the EEDF.

Rate coefficients for excitation from the ground vibrational state to symmetric modes ($v00$) for $v = 1$ to $v = 8$ and for $v = 10$ were calculated by employing the symmetric stretch excitation cross sections (shown in Fig. 1 and in its inset) in Eq. (2). The results of partial rate coefficients are shown in Fig. 6. Rate coefficients for (100) excitation exceed rates for excitation of other symmetric stretch levels for an order of magnitude due to large cross sections for this excitation channel. Due to the existence of the virtual part in (100) and (200) cross sections, rates for these states have onsets at low E/N values.

All these partial rate coefficients were summed to total rate coefficients and the results are presented in Fig. 7. The maxima are shifted to higher E/N values while descending and spreading at the same time with increasing the B/N value. Their location corresponds to the mean electron energy range of the resonance that appears in the vibrational cross-section dependence on electron energy at about 3.8 eV. The growth of the magnetic field has the effect of slowing down the electrons, keeping their mean energy more and more in the interval belonging to the resonance, which widens the peak region. Due to the reduced mean energy, higher E/N values are needed to reach the resonance energy region; hence the peaks are shifted. The decrease of maxima is a consequence of the shape of EEDFs for different B/N values—it is indicated that the number of electrons found in the resonance region drops with increasing B/N. This behavior is also reflected in rate coefficients for excitations of the bending (010), (020), and (040) modes (Fig. 8). An additional feature is observed in (010) excitation rates—the threshold peak in the cross-section dependence on electron energy, which has the greatest magnitude of all the vibrational cross sections in the low-energy part, noticeably affects the shape of rate coefficients to an increasing extent with the rise of the magnetic field. With the increase of the magnetic field, for the same E/N value, EEDFs tend to shift their bulk to low electron energies. For low E/N values this means that the mean electron energy is shifted more to the energy range of the threshold peak, which leads to its significant contribution to the rates in the low E/N interval. Rates are greater in magnitude than they would have

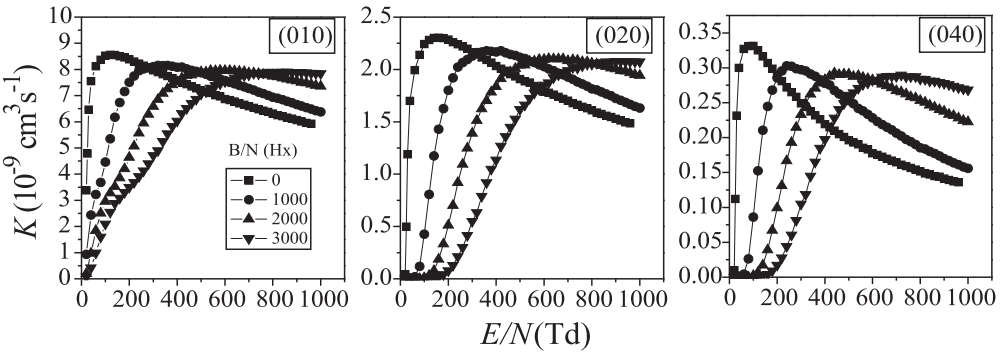

FIG. 8. Rate coefficients for bending vibrational mode excitation vs reduced electric field for different reduced magnetic field values.

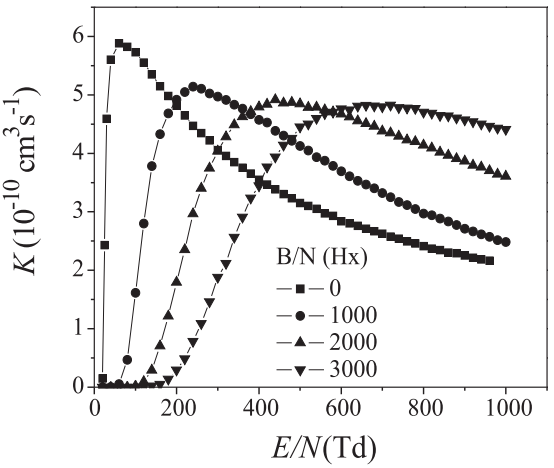

FIG. 9. Rate coefficients for the (120) vibrational mode excitation vs reduced electric field for different reduced magnetic field values.

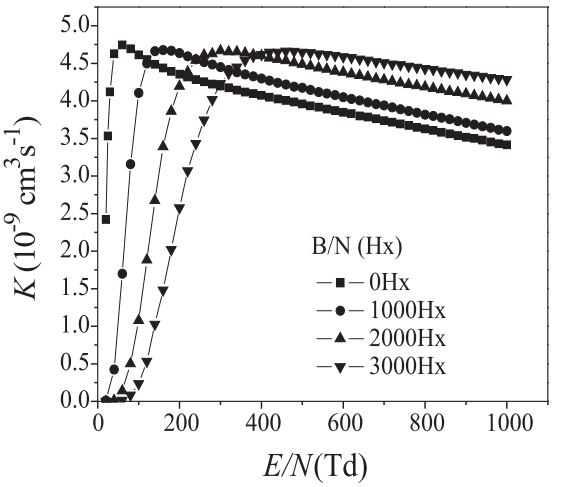

FIG. 10. Rate coefficients for the (001) vibrational mode excitation vs reduced electric field for different reduced magnetic field values.

been if there was no threshold peak. This is a general rule, but the position and the intensity of the threshold peak for the (010) state makes the (010) rates start rising much faster and sooner than the rates for other states considered in this paper. The onset of (010) rate coefficients is not shifted to higher E/N values even when the reduced magnetic field of 3000 Hx is applied. The influence of the magnetic field is weak up to about 200 Td, when it starts to rise.

A slight delay of the rates' onset appearing due to the influence of the magnetic field, which can be observed in the case of symmetric stretch modes, is hard to notice in the (010) mode. It is more pronounced in case of other bending modes, (020) and (040) and also in Fig. 9, representing rates for excitation of the combined (120) mode. This delay, however, is not so dramatic for the state (001) (see Fig. 10) and maxima are closer in position and magnitude than in the previous cases. As a consequence, with the inclusion of the magnetic field rate coefficients start to overcome those obtained in the absence of the magnetic field sooner than for the other states and the values are higher in a wider range of the given E/N values with an almost insignificant drop of maximal values as the reduced magnetic field value grows higher. Additionally, the shape of the (001) rates with nearly parallel lines for different B/N values indicates that rates for excitation of the (001) state rise with the increase of the magnetic field in a much wider range than rates for excitation of other vibrational levels. Interestingly, the behavior shown is caused by the existence of the intensive and wide threshold peak in CSs for excitation of this state. This peak mostly originates from the direct dipole scattering [28]. The described behavior of the (001) mode excitation rates with increase of the magnetic field is very convenient for the CO_2 conversion process, since the asymmetric stretch mode is the most important vibrational excitation channel leading to dissociation of this molecule [64]. Mean electron energy is maintained in the range of the vibrational excitation more efficiently with the presence of the magnetic field than in its absence. As vibrational excitation rate coefficients rise, the vibrational assisted dissociation rates also rise, which is very beneficial for CO_2 conversion.

IV. CONCLUSION

Rate coefficients for electron impact vibrational excitation of carbon dioxide in the presence of electric and magnetic fields were studied. A compilation of results for excitation to individual vibrational excitation levels was presented. The behavior of rate coefficients as a function of E/N and B/N values was discussed. The inclusion of the magnetic field has the effect of shifting rates in the scale of E/N. As a consequence, rate coefficients are increased in a wide E/N range. Since vibrational excitation is the main mechanism of CO_2 dissociation in nonequilibrium plasma, this increase implies the enhancement of CO_2 dissociation rates upon application of the magnetic field. The greater the magnetic field is, the greater the rate coefficients are. However, as the reduced magnetic field value rises, the region of the increase of vibrational rates moves towards higher E/N values. Therefore, one should find some compromise between these two tendencies in practical applications.

ACKNOWLEDGMENTS

This work was supported in part by the Ministry of Education, Science and Technological Development of the Republic of Serbia under Grant No. 171016.

M.M.V. and G.B.P. conceptualized the work; M.M.V, M.M.R., and V.V.S. performed calculations; M.M.V. wrote the paper and provided images; and G.B.P. and M.M.R. reviewed and edited the paper.

[1] O. Taylan and H. Berberoglu, Dissociation of carbon dioxide using a microhollow cathode discharge plasma reactor: Effects of applied voltage, flow rate and concentration, Plasma Sources Sci. Technol. **24**, 015006 (2015).

[2] G. J. van Rooij, D. C. M. van den Bekerom, N. den Harder, T. Minea, G. Berden, W. A. Bongers, R. Engeln, M. F. Graswinckel, E. Zoethout, and M. C. M. van de Sanden, Taming microwave plasma to beat thermodynamics in CO_2 dissociation, Faraday Discuss. **183**, 233 (2015).

[3] A. Bogaerts, T. Kozák, K. van Laer, and R. Snoeckx, Plasma-based conversion of CO_2: Current status and future challenges, Faraday Discuss. **183**, 217 (2015).

[4] T. Kozák and A. Bogaerts, Evaluation of the energy efficiency of CO_2 conversion in microwave discharges using a reaction kinetics model, Plasma Sources Sci. Technol. **24**, 015024 (2015).

[5] T. Silva, N. Britun, T. Godfroid, and R. Snyders, Optical characterization of a microwave pulsed discharge used for dissociation of CO_2, Plasma Sources Sci. Technol. **23**, 025009 (2014).

[6] L. D. Pietanza, G. Colonna, G. D'Ammando, A. Laricchiuta, and M. Capitelli, Vibrational excitation and dissociation mechanisms of CO_2 under non-equilibrium discharge and post-discharge conditions, Plasma Sources Sci. Technol. **24**, 042002 (2015).

[7] L. D. Pietanza, G. Colonna, G. D'Ammando, A. Laricchiuta, and M. Capitelli, Non equilibrium vibrational assisted dissociation and ionization mechanisms in cold CO_2 plasmas, Chem. Phys. **468**, 44 (2016).

[8] Q. Huang, D. Zhang, D. Wang, K. Liu, and A. W. Kleyn, Carbon dioxide dissociation in non-thermal radiofrequency and microwave plasma, J. Phys. D: Appl. Phys. **50**, 294001 (2017).

[9] A. Fridman, *Plasma Chemistry*, 2nd ed. (Cambridge University, Cambridge, England, 2008).

[10] L. D. Pietanza, G. Colonna, V. Laporta, R. Celiberto, G. D'Ammando, A. Laricchiuta, and M. Capitelli, Influence of electron molecule resonant vibrational collisions over the symmetric mode and direct excitation-dissociation cross sections of CO_2 on the electron energy distribution function and dissociation mechanisms in cold pure CO_2 plasmas, J. Phys. Chem. A **120**, 2614 (2016).

[11] G. B. Poparić, M. M. Ristić, and D. S. Belić, Electron energy transfer rate coefficients of carbon dioxide, J. Phys. Chem. A **114**, 1610 (2010).

[12] S. N. Abolmasov, Physics and engineering of crossed-field discharge devices, Plasma Sources Sci. Technol. **21**, 035006 (2012).

[13] K. Arita and S. Iizuka, Production of CH_4 in a low-pressure CO_2/H_2 discharge with magnetic field, J. Mater. Sci. Chem. Eng. **3**, 69 (2015).

[14] J. Annaloro, A. Bultel, and P. Omaly, Detailed kinetic of CO_2 dissociation and C ionization: Application to atmospheric martian entries, J. Phys: Conf. Ser. **511**, 012053 (2014).

[15] M. Vojnović, M. Popović, M. M. Ristić, M. D. Vićić, and G. B. Poparić, Rate coefficients for electron impact excitation of CO, Chem. Phys. **423**, 1 (2013).

[16] M. Vojnović, M. Popović, M. M. Ristić, M. D. Vićić, and G. B. Poparić, Rate coefficients for electron impact excitation of N_2, Chem. Phys. **463**, 38 (2015).

[17] M. A. Ridenti, L. L. Alves, V. Guerra, and J. Amorim, The role of rotational mechanisms in electron swarm parameters at low reduced electric field in N_2, O_2, and H_2, Plasma Sources Sci. Technol. **24**, 035002 (2015).

[18] M. Grofulović, L. L. Alves, and V. Guerra, Electron-neutral scattering cross sections for CO_2: A complete and consistent set and an assessment of dissociation, J. Phys. D: Appl. Phys. **49**, 395207 (2016).

[19] M. M. Ristić, Excitation of the H_2, N_2 and CO molecules by low energy electrons, Ph.D. thesis, University of Belgrade, 2011.

[20] M. M. Vojnović, Rate coefficients for electron impact excitation and ionization of CO and N_2 molecules in the presence of electric and magnetic fields, Ph.D. thesis, University of Belgrade, 2016.

[21] A. Bourdon, J. Annaloro, A. Bultel, M. Capitelli, G. Colonna, A. Guy, T. Magin, M. P. A. Munafó, and L. Pietanza, Reduction of state-to-state to macroscopic models for hypersonics, Open Plasma Phys. J. **7**, 60 (2014).

[22] R. D. White, K. F. Ness, R. E. Robson, and B. Li, Charged-particle transport in gases in electric and magnetic fields crossed at arbitrary angles: Multiterm solution of Boltzmann's equation, Phys. Rev. E **60**, 2231 (1999).

[23] A. M. Nolan, M. J. Brennan, K. F. Ness, and A. B. Wedding, A benchmark model for analysis of electron transport in non-conservative gases, J. Phys. D: Appl. Phys. **30**, 2865 (1997).

[24] G. J. M. Hagelaar and L. C. Pitchford, Solving the Boltzmann equation to obtain electron transport coefficients and rate coefficients for fluid models, Plasma Sources Sci. Technol. **14**, 722 (2005).

[25] Y. Itikawa, Cross sections for electron collisions with carbon dioxide, J. Phys. Chem. Ref. Data **31**, 749 (2002).

[26] M. T. Lee and V. McKoy, Cross sections for electron impact excitation of the low-lying electron states of CO_2, J. Phys. B: At. Mol. Phys. **16**, 657 (1983).

[27] C. H. Lee, C. Winstead, and V. McKoy, Collisions of low-energy electrons with CO_2, J. Chem. Phys. **111**, 5056 (1999).

[28] K. H. Kochem, W. Sohn, N. Hebel, K. Jung, and H. Ehrhardt, Elastic electron scattering and vibrational excitation of CO_2 in the threshold energy region, J. Phys. B: At. Mol. Phys. **18**, 4455 (1985).

[29] H. Tanaka, T. Ishikawa, T. Masai, T. Sagara, L. Boesten, M. Takekawa, Y. Itikawa, and M. Kimura, Elastic collisions of low- to intermediate-energy electrons from carbon dioxide: Experimental and theoretical differential cross sections, Phys. Rev. A **57**, 1798 (1998).

[30] I. Kanik, D. C. McCollum, and J. C. Nickel, Absolute elastic differential scattering cross sections for electron impact on carbon dioxide in the intermediate energy region, J. Phys. B: At. Mol. Phys. **22**, 1225 (1989).

[31] H. Kawahara, H. Kato, M. Hoshino, H. Tanaka, L. Campbell, and M. J. Brunger, Integral cross sections for electron impact excitation of the $^1\Sigma_u+$ and $^1\Pi_u$ electronic states in CO_2, J. Phys. B: At. Mol. Phys. **41**, 085203 (2008).

[32] M. A. Green, P. J. O. Teubner, L. Campbell, M. J. Brunger, M. Hoshino, T. Ishikawa, M. Kitajima, H. Tanaka, Y. Itikawa, M. Kimura, and R. J. Buenker, Absolute differential cross sections for electron impact excitation of the 10.8–11.5 eV energy-loss states of CO_2, J. Phys. B: At. Mol. Phys. **35**, 567 (2002).

[33] K. N. Klump and E. N. Lassettre, Generalized oscillator strengths for two transitions in CO_2 at incident electron energies of 300, 400 and 500 eV, Electron Spectrosc. Relat. Phenom. **14**, 215 (1978).

[34] V. Laporta, J. Tennyson, and R. Celiberto, Calculated low-energy electron-impact vibrational excitation cross sections for CO_2 molecule, Plasma Sources Sci. Technol. **25**, 06LT02 (2016).

[35] Y. Nakamura, Drift velocity and longitudinal diffusion coefficient of electrons in CO_2-Ar mixtures and electron collision cross sections for CO_2 molecules, Aust. J. Phys. **48**, 357 (1995).

[36] M. Kitajima, S. Watanabe, H. Tanaka, M. Takekawa, M. Kimura, and Y. Itikawa, Differential cross sections for vibrational excitation of CO_2 by 1.5–30 eV electrons, J. Phys. B: At. Mol. Phys. **34**, 1929 (2001).

[37] L. Campbell, M. J. Brunger, and T. N. Rescigno, Carbon dioxide electron cooling rates in the atmospheres of Mars and Venus, J. Geophys. Res. **113**, E08008 (2008).

[38] C. W. McCurdy, W. A. Isaacs, H.-D. Meyer, and T. N. Rescigno, Resonant vibrational excitation of CO_2 by electron impact: Nuclear dynamics on the coupled components of the $^2\Pi_u$ resonance, Phys. Rev. A **67**, 042708 (2003).

[39] R. D. Hake, Jr. and A. V. Phelps, Momentum-transfer and inelastic-collision cross sections for electrons in O_2, CO, and CO_2, Phys. Rev. **158**, 70 (1967).

[40] B. G. Lindsay and M. A. Mangan, in *Photon and Electron Interactions with Atoms, Molecules and Ions*, edited by Y. Itikawa, Elementary Particles, Nuclei and Atoms Vol. 17C (Springer, Berlin, 2003).

[41] D. Rapp and D. D. Briglia, Total cross sections for ionization and attachment in gases by electron impact. II. Negative-ion formation, J. Chem. Phys. **43**, 1480 (1965).

[42] L. S. Polak and D. I. Slovetsky, Electron impact induced electronic excitation and molecular dissociation, Int. J. Radiat. Phys. Chem. **8**, 257 (1976).

[43] M. Allan, Vibrational structures in electron-CO_2 scattering below the $^2\Pi_u$ shape resonance, J. Phys. B: At. Mol. Phys. **35**, L387 (2002).

[44] W. M. Johnstone, P. Akther, and W. R. Newell, Resonant vibrational excitation of carbon dioxide, J. Phys. B: At. Mol. Phys. **28**, 743 (1995).

[45] H. C. Straub, B. G. Lindsay, K. A. Smith, and R. F. Stebbings, Absolute partial cross sections for electron-impact ionization of CO_2 from threshold to 1000 eV, J. Chem. Phys. **105**, 4015 (1996).

[46] H. T. Saelee, J. Lucas, and J. W. Limbeek, Time-of-flight measurement of electron drift velocity and longitudinal diffusion coefficient in nitrogen, carbon monoxide, carbon dioxide and hydrogen, IEE J. Solid-State Electron Devices **1**, 111 (1977).

[47] W. Roznerski and K. Leja, Electron drift velocity in hydrogen, nitrogen, oxygen, carbon monoxide, carbon dioxide and air at moderate E/N, J. Phys. D: Appl. Phys. **17**, 279 (1984).

[48] M. T. Elford, The drift velocity of electrons in carbon dioxide at 293°K, Aust. J. Phys. **19**, 629 (1966).

[49] J. L. Hernández-Ávila, E. Basurto, and J. de Urquijo, Electron transport and swarm parameters in CO_2 and its mixtures with SF_6, J. Phys. D: Appl. Phys. **35**, 2264 (2002).

[50] H. Hasegawa, H. Date, M. Shimozuma, K. Yoshida, and H. Tagashira, The drift velocity and longitudinal diffusion coefficient of electrons in nitrogen and carbon dioxide from 20 to 1000 Td, J. Phys. D: Appl. Phys. **29**, 2664 (1996).

[51] M. Vass, I. Korolov, D. Loffhagen, N. Pinhão, and Z. Donkó, Electron transport parameters in CO_2: Scanning drift tube measurements and kinetic computations, Plasma Sources Sci. Technol. **26**, 065007 (2017).

[52] C. S. Lakshminarasimha, J. Lucas, and N. Kontoleon, Diffusion and ionization studies for electron swarms in carbon monoxide and carbon dioxide, J. Phys. D: Appl. Phys. **7**, 2545 (1974).

[53] Y. K. Deng and D. M. Xiao, Effective ionization coefficients and electron drift velocities in gas mixtures of CF_3I with N_2 and CO_2 obtained from Boltzmann equation analysis, Chin. Phys. B **22**, 035101 (2013).

[54] J. S. Townsend, The conductivity produced in gases by the aid of ultra-violet light, Philos. Mag. **3**, 557 (1902).

[55] M. S. Bhalla and J. D. Craggs, Measurement of ionization and attachment coefficients in carbon dioxide in uniform fields, Proc. Phys. Soc. **76**, 369 (1960).

[56] H. Schlumbohm, Stoßionisierungskoeffizient α, mittlere elektronenenergien und die beweglichkeit von elektronen in gasen, Z. Phys. **184**, 492 (1965).

[57] M. Yousfi, J. de Urquijo, A. Juárez, E. Basurto, and J. L. Hernández-Ávila, Electron swarm coefficients in CO_2–N_2 and CO_2–O_2 mixtures, IEEE T. Plasma Sci. **37**, 764 (2009).

[58] P. A. Chatterton and J. D. Craggs, Attachment coefficient measurements in carbon dioxide, carbon monoxide, air and helium-oxygen mixtures, Proc. Phys. Soc. **85**, 355 (1965).

[59] H. N. Kucukarpaci and J. Lucas, Simulation of electron swarm parameters in carbon dioxide and nitrogen for high E/N, J. Phys. D: Appl. Phys. **12**, 2123 (1979).

[60] W. Roznerski and J. Mechlińska-Drewko, The ratio of lateral diffusion coefficient to mobility for electrons in oxygen and carbon dioxide, J. Phys. Colloques **40**, C7-149 (1979).

[61] W. Roznerski and J. Mechlińska-Drewko, Ratio of the lateral diffusion coefficient to the mobility for electrons in carbon monoxide and carbon dioxide, Phys. Lett. A **70**, 271 (1979).

[62] P. Chantry, Final Technical Report ARPA, Techical Report Order No. 3342, Harvard-Smithsonian Centre for Astrophysics, 1978.

[63] D. S. Belić, Field effects on dielectronic recombination rate coefficients of Mg^+ ions, Chem. Phys. **130**, 141 (1989).

[64] T. Kozák and A. Bogaerts, Splitting of CO_2 by vibrational excitation in non-equilibrium plasmas: A reaction kinetics model, Plasma Sources Sci. Technol. **23**, 045004 (2014).